Supporting Information for:

Temperature Dependence of the Hydrated Electron's g-Factor and Persistence of a Cavity-Localized Electron at Elevated Temperature

Ar. M. Fonlon, Christopher J. Mundy, and John M. Herbert*

[1] *Department of Chemistry & Biochemistry*
The Ohio State University, Columbus, Ohio 43210 USA
[2] *Physical Science Division, Pacific Northwest National Laboratory*
Richland, Washington 99352 USA

August 17, 2026

Contents

*herbert@chemistry.ohio-state.edu

References

[1] Flyvbjerg, H.; Peterson, H. G. Error estimates on averages of correlated data. *J. Chem. Phys.* **1989,** *91,* 461–466.

[2] Herbert, J. M.; Jacobson, L. D. Structure of the aqueous electron: Assessment of one-electron pseudopotential models in comparison to experimental data and time-dependent density functional theory. *J. Phys. Chem. A* **2011,** *115,* 14470–14483.

[3] Uhlig, F.; Herbert, J. M.; Coons, M. P.; Jungwirth, P. Optical spectroscopy of the bulk and interfacial hydrated electron from ab initio calculations. *J. Phys. Chem. A* **2014,** *118,* 7507–7515.

[4] Baer, R.; Livshits, E.; Salzner, U. Tuned range-separated hybrids in density functional theory. *Annu. Rev. Phys. Chem.* **2010,** *61,* 85–109.

[5] Park, S. J.; Schwartz, B. J. Understanding the temperature dependence and finite size effects in ab initio MD simulations of the hydrated electron. *J. Chem. Theory Comput.* **2022,** *18,* 4973–4982.

[6] Mandal, A.; Herbert, J. M. Simplified tuning of long-range corrected time-dependent density functional theory. *J. Phys. Chem. Lett.* **2025,** *16,* 2672–2680.

S1 Block-Averaging Procedure

Block averaging was performed using the Flyvbjerg-Peterson technique.[1] In what follows, N_{block} is the block size and n_{block} is the number of blocks in each block level. The procedure involves choosing N_{block} by testing various blockings and determining convergence in the standard error of the mean (SEM),

$$\text{SEM} = \frac{\sigma}{\sqrt{n_{\text{block}}}} \,. \tag{S1}$$

Here, σ is the standard deviation of the mean. Starting with a given data set with n_{block} data points, the mean and SEM are computed across all n_{block}. The resulting means are then used as a starting point for the next iteration and block level, in which the means of consecutive pairs in this set are computed along with SEMs, resulting in a block size of $n_{\text{block}}/2$ at this level. This process iterates until $n_{\text{block}} < 2$. Convergence in the SEM across each blocking iteration (N_{block}) is used to determine which level of block-averaging is sufficient. In the case of lack of convergence in the SEM, a block level with $n_{\text{block}} \geq 10$ is chosen and a lower-bound estimate to the SEM is reported. Table S1 shows the block sizes selected for each averaged quantity and indicates whether the SEM reported in Table S2 is a lower-bound estimate. Table S2 contains block-averaged data corresponding to the quantities in Table 2, the latter of which provides conventional averages and standard deviations.

S2 Additional Data Tables

Table S1: Block sizes and indicated convergence of the SEM.

T (K)	$\langle r_{\mathrm{HB}} \rangle$	$\langle r_{\mathrm{gyr}} \rangle$	$\langle n_{\mathrm{HB}} \rangle$	$\langle n_2 \rangle$	$\langle \Delta g \rangle$
273	512 / yes	256 / no	128 / yes	1024 / no	256 / yes
300	512 / yes	256 / no	512 / no	1024 / no	256 / no
338	512 / yes	256 / no	512 / no	1024 / no	256 / no
373	128 / yes	256 / no	512 / no	1024 / no	256 / no

Table S2: Block-averaged properties of e^-(aq) from *ab initio* MD simulations.[a]

T (K)	$\langle r_{\mathrm{HB}} \rangle$[b] (Å)	$\langle r_{\mathrm{gyr}} \rangle$[c] (Å)	$\langle n_{\mathrm{HB}} \rangle$[d]	$\langle n_2 \rangle$[e]	$\langle \Delta g \rangle$ (ppm)[f]
273	1.350 ± 0.413	2.415 ± 0.008[g]	3.997 ± 0.001	24.628 ± 0.080[g]	−1487 ± 4
300	1.383 ± 0.511	2.396 ± 0.013[g]	4.319 ± 0.050[g]	22.917 ± 0.166[g]	−1557 ± 9[g]
338	1.350 ± 0.517	2.484 ± 0.020[g]	4.204 ± 0.040[g]	18.829 ± 0.220[g]	−1598 ± 9[g]
373	1.383 ± 0.591	2.487 ± 0.018[g]	4.213 ± 0.024[g]	18.639 ± 0.166[g]	−1659 ± 10[g]

[a] Error bars are SEMs, computed using 120 ps of simulation data at each temperature, using block sizes provided in Table S1. For standard deviations, see Table 2. [b] From a Gaussian fit of the first peak in $G_{\mathrm{eH}}(r)$. [c] Eq. 3, computed for the SOMO using QM/MM snapshots. [d] Number of hydrogen atoms in the first solvation shell of e^-(aq); see Fig. S3. [e] Number of oxygen atoms in the first two solvation shells of e^-(aq); see Fig. S4. [f] Computed from QM/MM snapshots. [g] Indicates a lower-bound estimate to the SEM, as described in Section S1.

S3 Additional Figures

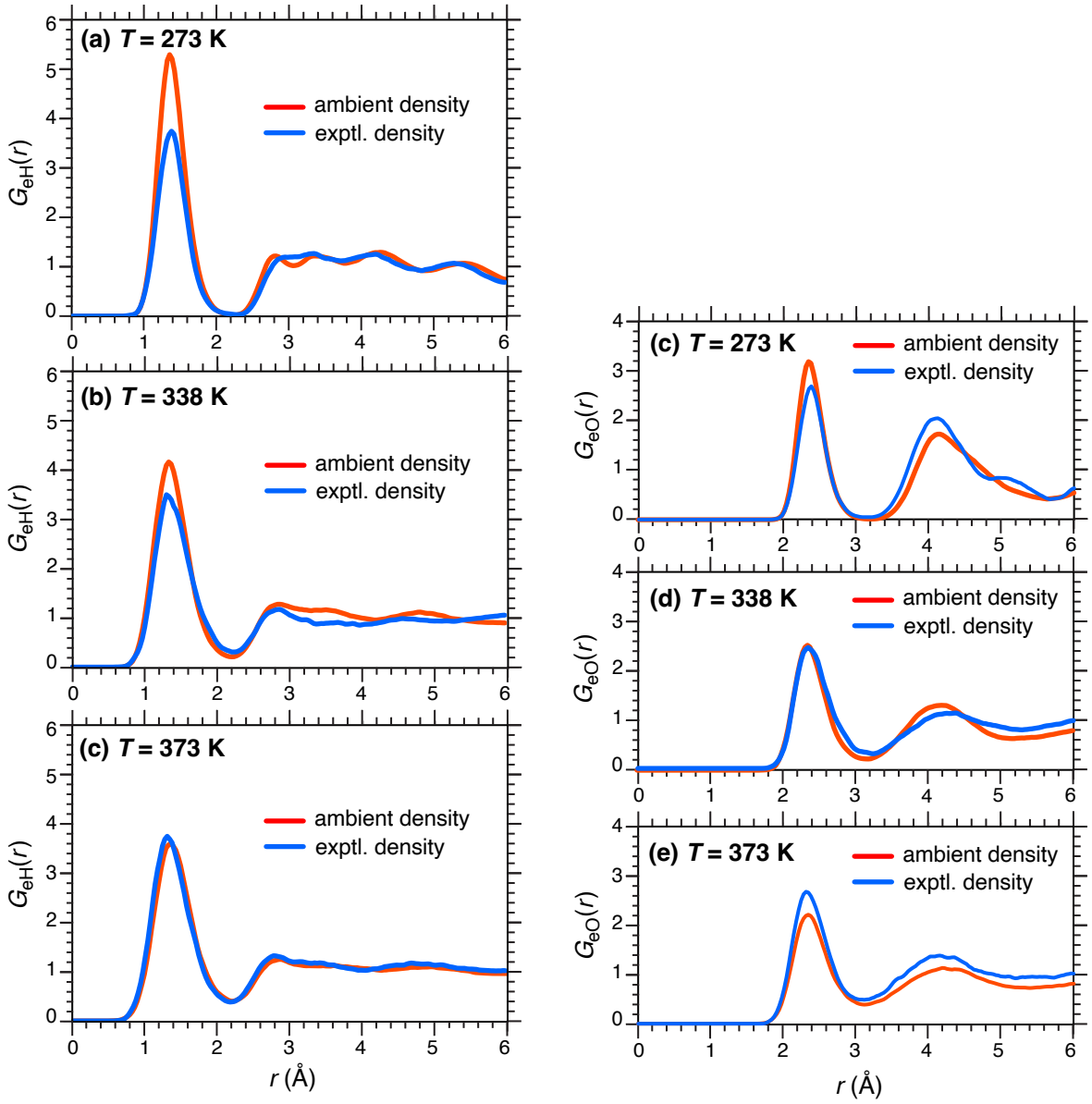

Figure S1: RDFs $G_{\mathrm{eH}}(r)$ (left column) and $G_{\mathrm{eO}}(r)$ (right column) at three different temperatures, comparing results from simulations at ambient density (0.997 g/cm^3, as in Fig. 2) to those performed using the experimental density of neat liquid water at the indicated temperature. (Simulations at $T = 300$ K use the experimental density, so that comparison is not shown.) The ambient-density simulations use 120 ps of averaging whereas the experimental density simulations use only 30 ps.

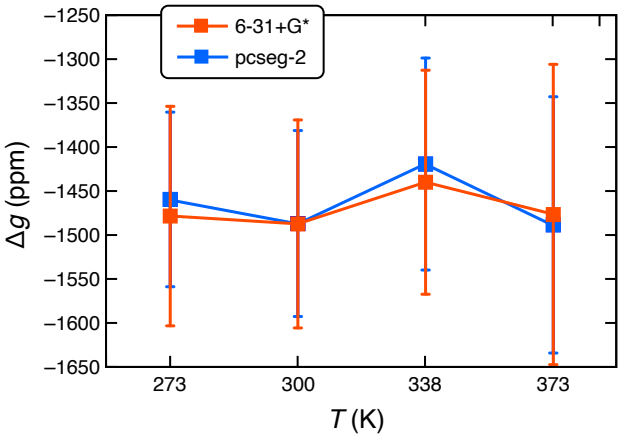

Figure S2: Basis-set comparison for Δg calculations. Shown are the mean values of Δg, averaged over 10 ps of simulation data at each temperature, with whiskers representing one standard deviation above and below the mean. These data correspond to the first 10 ps of Fig. 4a, so the temperature effect is not reproduced as it requires at least 40–50 ps of sampling. However, these data do demonstrate that basis-set effects on Δg are small.

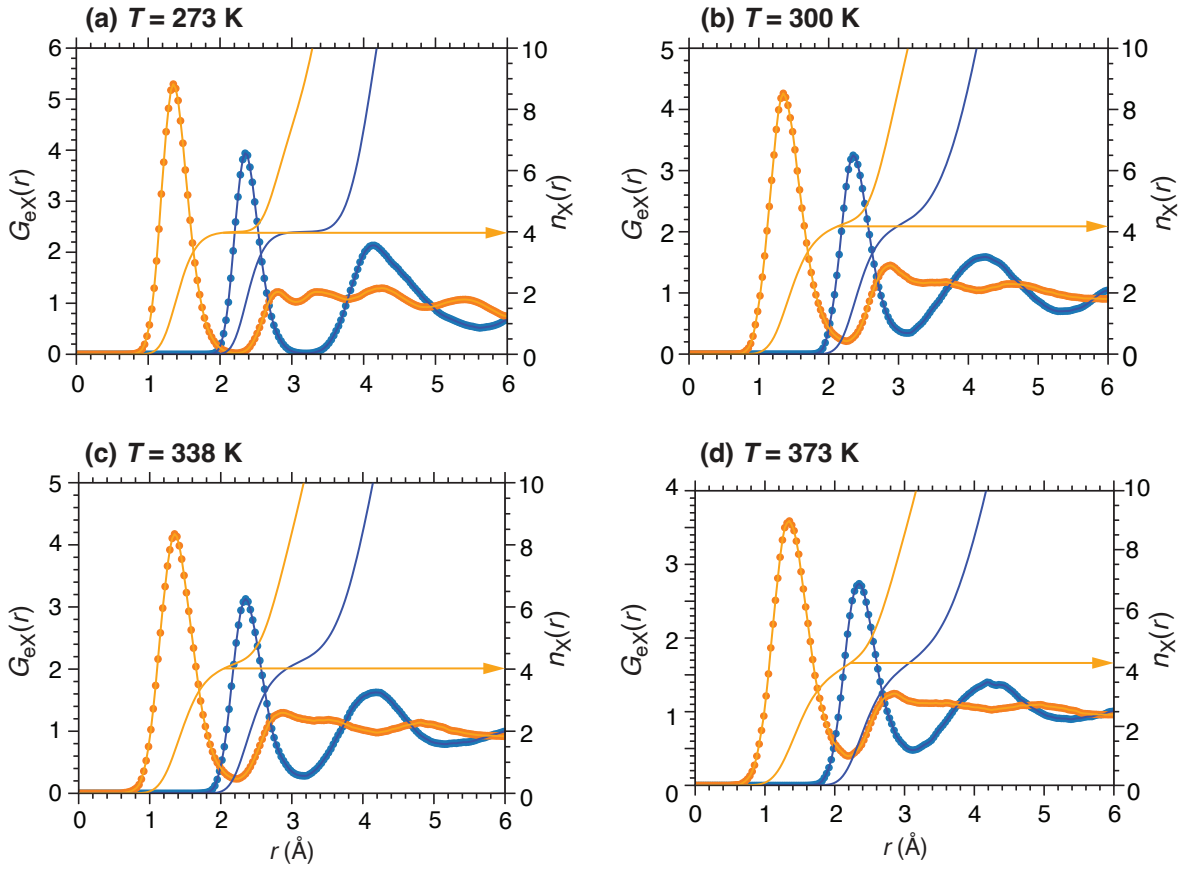

Figure S3: RDFs $G_{\mathrm{eX}}(r)$ at various temperatures (for X = O or H), to be read from the scale on the left in each panel. Integrated coordination numbers $n_{\mathrm{X}}(r)$ are also plotted, to be read from the scale on the right. The value of $\langle n_{\mathrm{HB}} \rangle$ is read from the first local minimum of $G_{\mathrm{eH}}(r)$, as indicated by the horizontal arrow.

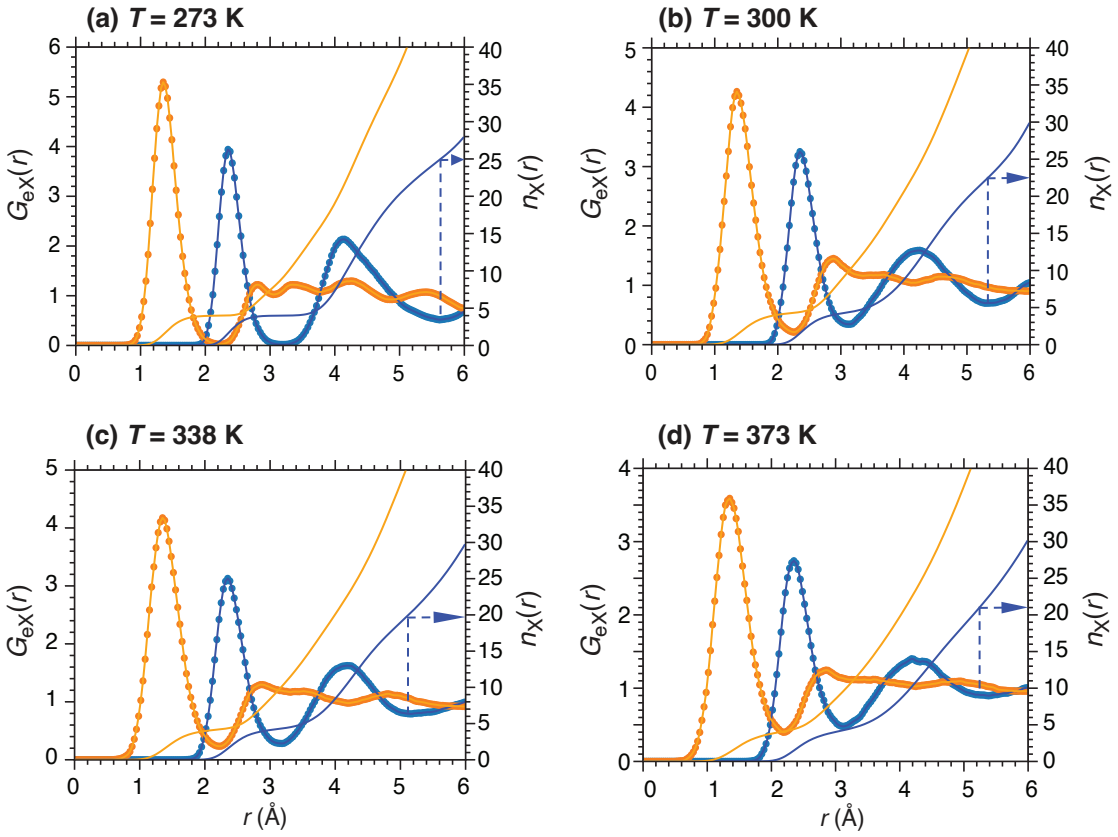

Figure S4: RDFs $G_{\mathrm{eX}}(r)$ at various temperatures (for X = O or H), to be read from the scale on the left in each panel. Integrated coordination numbers $n_{\mathrm{X}}(r)$ are also plotted, to be read from the scale on the right. (These data are the same as those in Fig. S3 but the $n_{\mathrm{X}}(r)$ axis is plotted on a different scale.) The value of $\langle n_2 \rangle$ is read from the second local minimum of $G_{\mathrm{eO}}(r)$, as indicated by the horizontal arrow.

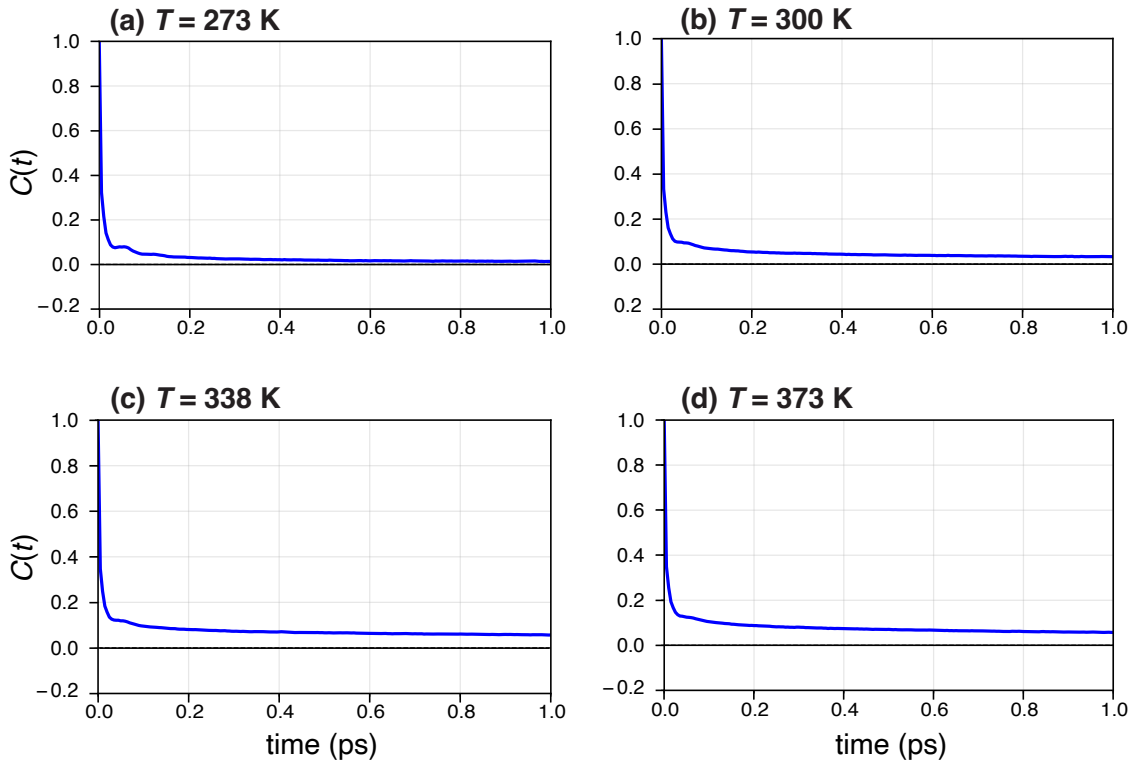

Figure S5: Autocorrelation functions $\langle \mathbf{v}(t) \cdot \mathbf{v}(0) \rangle$ for the H_2O angle bisector $\mathbf{v}(t)$ at various temperatures, indicating significant librational dynamics even at $T = 273$ K where the RDFs suggest a well-defined shell structure where water exchange may be frozen out.

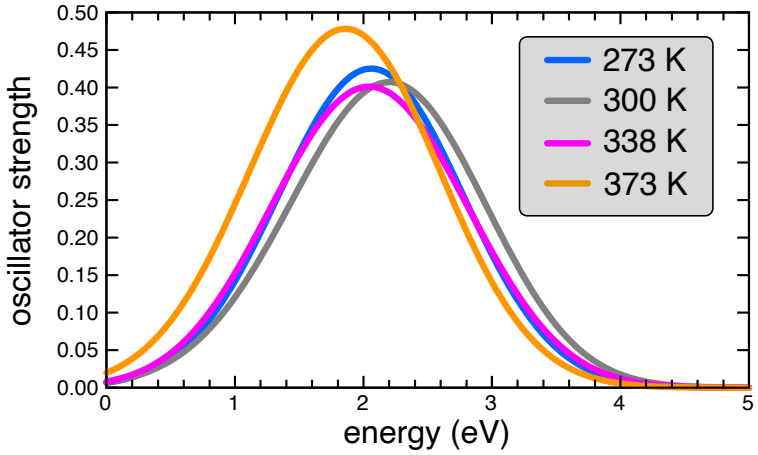

Figure S6: Electronic absorption spectra of e^-(aq), obtained from time-dependent (TD-)DFT calculations on snapshots from the simulation data. Each spectrum was computed from 100 snapshots using a QM/MM setup as described in Section 2.3, except that the QM radius was limited to 5 Å, as in other similar calculations of the e^-(aq) absorption spectrum.[2,3] (This procedure affords 19 ± 2 QM water molecules at each temperature, except for $T = 373$ K where it affords 17 ± 2.) TD-DFT calculations were performed at the LRC-ωPBE/6-31++G* level, using a range-separation parameter $\omega = 0.20$ bohr^{-1} that was determined via optimal tuning (see Fig. S7).[4] Three excited states were included for each snapshot and were broadened using a 0.6 eV Gaussian. The absorption spectrum shifts non-monotonically with temperature, which was also observed in similar calculations that were reported in Ref. 5.

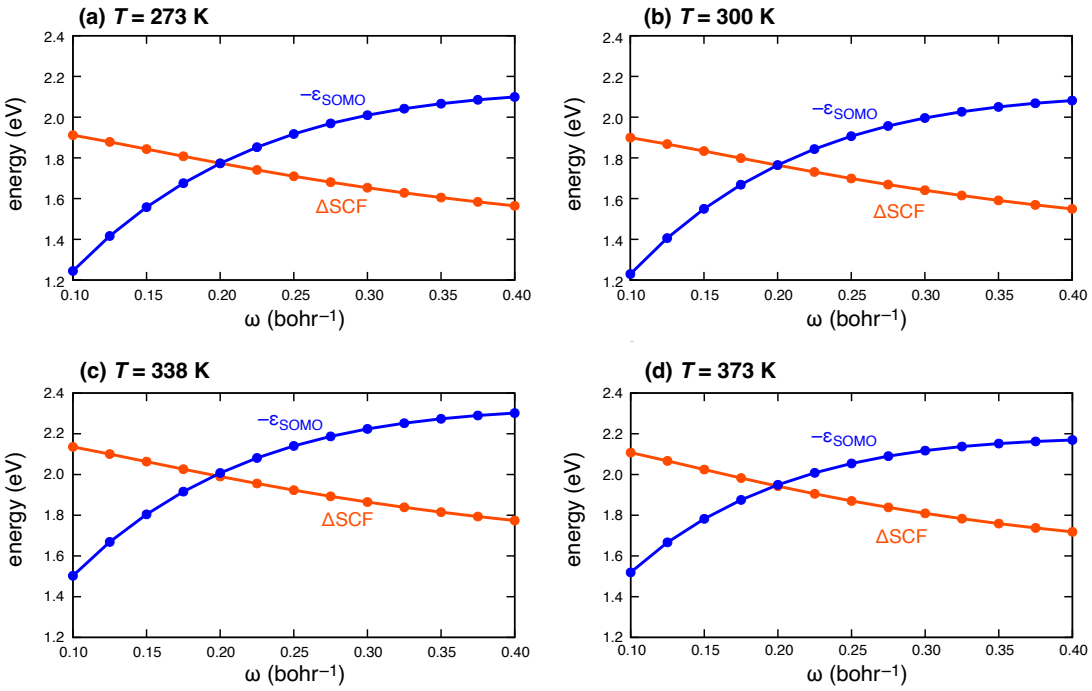

Figure S7: Tuning plots for QM/MM snapshots at the LRC-ωPBE/6-31++G* level using a 5 Å QM radius. In each case, both $\varepsilon_{\mathrm{SOMO}}(\omega)$ and $\mathrm{IE}(\omega)$ are averaged over 100 snapshots, leading to an optimized value $\omega = 0.20$ bohr^{-1} that is used to compute the spectra in Fig. S6. For comparison, the tuned value obtained with global density-dependent (GDD) tuning[6] is $\omega_{\mathrm{GDD}} = 0.26$ bohr^{-1}.

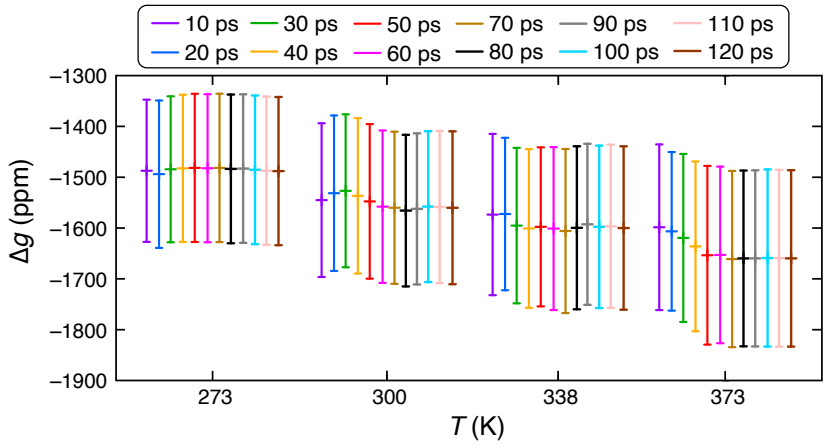

Figure S8: Cumulative averages of Δg over 10–120 ps, reversing the order of the data (so that $t = 0$ is the last snapshot in the trajectory). Otherwise, the procedure is the same as that used to obtain the similar averages (based on forward-time data) that are plotted in Fig. 4a.

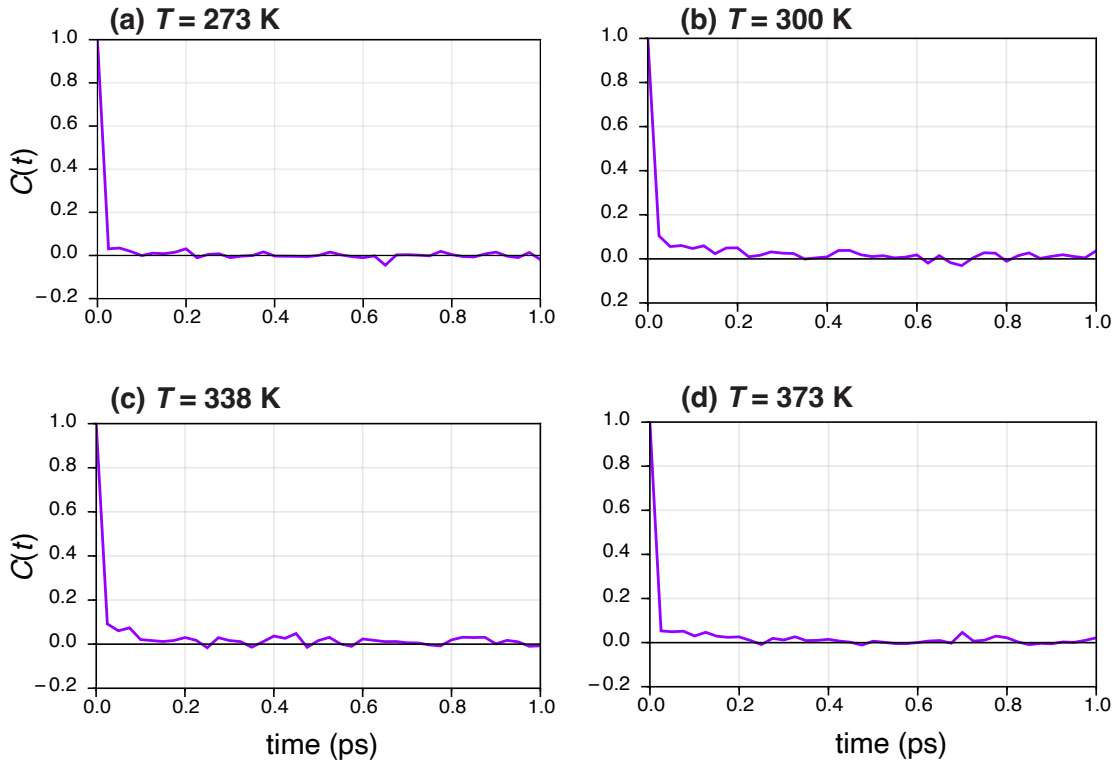

Figure S9: Autocorrelation functions for the spin density at each oxygen nucleus, for which static probability distributions are given in Fig. 7. Fits to single-exponential decay afford time constants of (a) 7 fs, (b) 12 fs, (c) 11 fs, and (d) 9 fs.

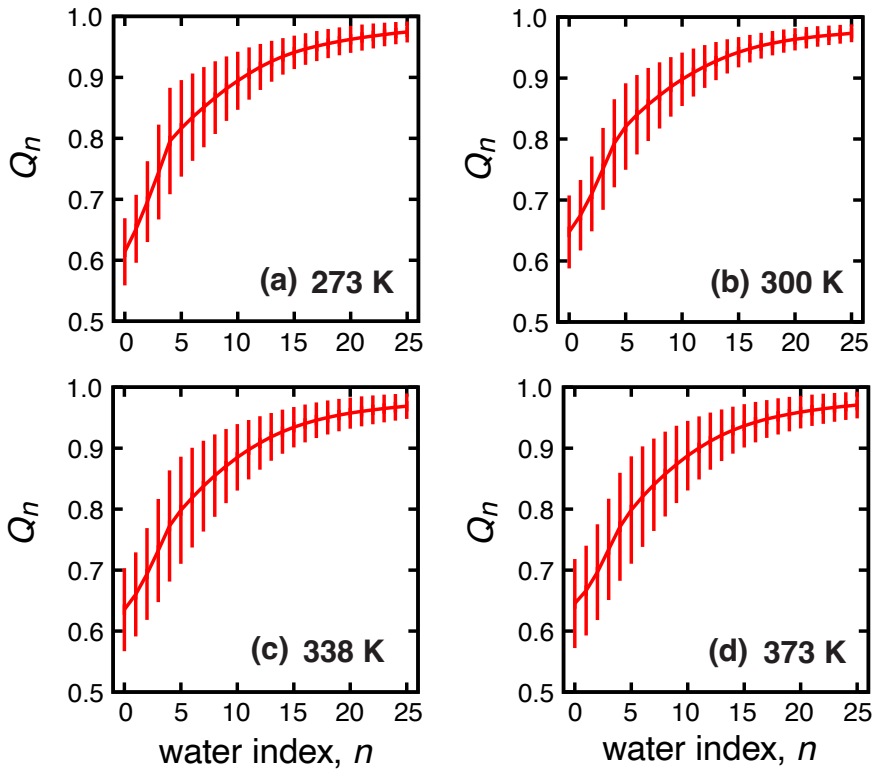

Figure S10: Cumulative spin charges Q_n (eq. 4) computed using Mulliken population analysis. Starting with the ghost atom ($Q_0 = q_{\mathrm{Gh}}$), Q_n accumulates each $q_{\mathrm{W}n}$ in order of increasing distance from the ghost atom, which is located at the instantaneous centroid of the SOMO. A curve connects the ensemble-averaged value $\langle Q_n \rangle$ at each n, with whiskers at each n representing one standard deviation above and below the mean. Calculations were performed at the PBEh(40)-rVV10/6-31+G* level using the QM/MM scheme that is described in Section 2 .3. These data should be compared to the analogous plot in Fig. 5 that is obtained using Becke population analysis rather than Mulliken analysis.

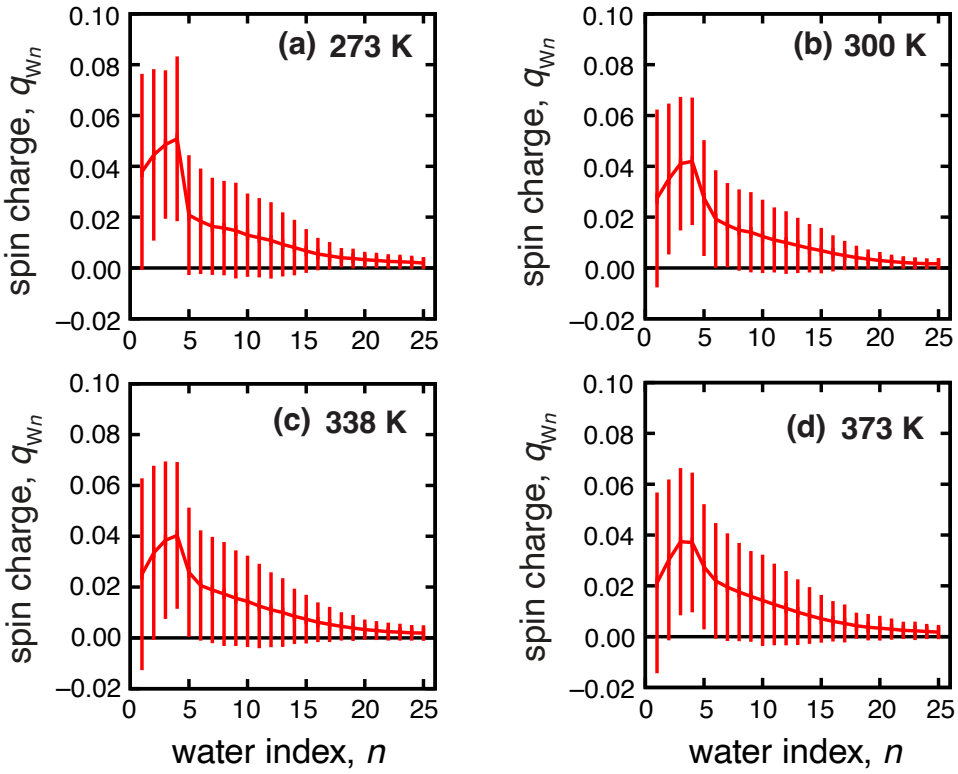

Figure S11: Spin charge $q_{\mathrm{W}n}$ on each water molecule, computed using Mulliken population analysis. By definition, $q_{\mathrm{W}n}$ is the spin charge on the nth nearest water molecule to the ghost atom that is located at the instantaneous centroid of the SOMO. A curve connects the ensemble-averaged value $\langle q_{\mathrm{W}n} \rangle$ at each n, with whiskers indicating one standard deviation above and below the mean. Calculations were performed at the PBEh(40)-rVV10/6-31+G* level using the QM/MM scheme described in Section 2.3. These data should be compared to the analogous plot in Fig. 6 that is obtained using Becke population analysis rather than Mulliken analysis.